PHYSICAL REVIEW D **84,** 103517 (2011)

Dark matter annihilation signatures from electroweak bremsstrahlung

Nicole F. Bell,[1] James B. Dent,[2] Thomas D. Jacques,[1,2] and Thomas J. Weiler[3]

[1]*School of Physics, The University of Melbourne, Victoria 3010, Australia*

[2]*Department of Physics and School of Earth and Space Exploration, Arizona State University, Tempe, Arizona 85287-1404, USA*

[3]*Department of Physics and Astronomy, Vanderbilt University, Nashville, Tennessee 37235, USA*

(Received 18 May 2011; published 16 November 2011)

We examine observational signatures of dark matter (DM) annihilation in the Milky Way arising from electroweak bremsstrahlung contributions to the annihilation cross section. It has been known for some time that photon bremsstrahlung may significantly boost DM annihilation yields. Recently, we have shown that electroweak bremsstrahlung of W and Z gauge bosons can be the dominant annihilation channel in some popular models with helicity-suppressed $2 \to 2$ annihilation. W/Z-bremsstrahlung is particularly interesting because the gauge bosons produced via annihilation subsequently decay to produce large correlated fluxes of electrons, positrons, neutrinos, hadrons (including antiprotons) and gamma rays, which are all of importance in indirect DM searches. Here, we calculate the spectra of stable annihilation products produced via $\gamma/W/Z$-bremsstrahlung. After modifying the fluxes to account for the propagation through the Galaxy, we set upper bounds on the annihilation cross section via a comparison with observational data. We show that stringent cosmic ray antiproton limits preclude a sizable DM contribution to observed cosmic ray positron fluxes in the class of models for which the bremsstrahlung processes dominate.

DOI: 10.1103/PhysRevD.84.103517 PACS numbers: 95.35.+d, 12.15.Lk, 95.85.Ry

I. INTRODUCTION

It has been firmly established that a significant fraction of the energy density of the Universe resides in the form of dark matter (DM), whose total abundance and approximate distribution has been inferred via its gravitational influence [1–3]. However, we have as yet no direct detection, and the fundamental particle properties of DM remain unknown. A promising technique to explore the particle nature of DM is to search for signatures of DM annihilation or decay. This is achieved by examining fluxes of particles emanating from regions of DM concentration either in our own Galaxy or throughout the cosmos.

Indirect DM detection has been the subject of much recent attention, due to measured cosmic ray excesses of positrons and electrons above those expected from conventional astrophysical processes. PAMELA has observed a sharp excess in the $e^+/(e^- + e^+)$ fraction at energies beyond approximately 10 GeV [4], without a corresponding excess in the antiproton/proton data [5,6], while Fermi and HESS have reported more modest excesses in the $(e^- + e^+)$ flux at energies of order 1 TeV [7,8]. These signals have led to a reexamination of positron production in nearby pulsars [9,10], emission from supernova remnants [11], acceleration of e^+e^- in cosmic ray sources [12], and propagation in conventional cosmic ray models [13]. Alternatively, it has been proposed the excess electrons and positrons are not due to conventional astrophysics process, but arise instead from DM annihilation or decay in the Galactic halo. A plethora of DM models have been designed with this goal in mind (for a review, see, for example, [14], and references therein).

A viable resolution of the cosmic ray $e^\pm$ data by means of DM annihilation requires a large branching ratio to leptons. A large branching ratio to hadrons would make a contribution to cosmic ray antiproton fluxes, for which stringent observational bounds exist. Therefore, so called leptophilic models are preferred, in which DM couples (at tree level) only to leptons. However, for many scenarios in which the DM particle is a Majorana fermion, annihilation to light fermions is helicity-suppressed ($\propto m_f^2/s$) in the s-wave contribution, and of course, velocity suppressed ($\propto v_{\rm DM}^2$) in the p-wave contribution. This is the case for popular DM candidates such as the neutralino of supersymmetric models, if $\sqrt{s} \sim 2M_{\rm DM}$ is below the W^+W^- threshold; or Bino models with highly suppressed annihilation to W^+W^- and ZZ final states. Large boost factors would be required for such a scenario to explain any observed positron excess.

It has long been known that photon bremsstrahlung can lift helicity suppressions [15–17]. We have recently shown that helicity suppressions are also lifted by the bremsstrahlung of a W or Z gauge boson [18,19] (see also [20]). (Electroweak radiative corrections to DM annihilation, but without the observation of helicity unsuppression, have been discussed in Refs. [21–28].) Where a helicity suppression is lifted, the cross sections for $\chi\chi \to \ell\bar{\ell}\gamma$, $\chi\chi \to \ell\bar{\ell}Z$, and $\chi\chi \to \ell\nu W$ can all greatly exceed that for the lowest-order process $\chi\chi \to \ell\bar{\ell}$. The bremsstrahlung processes thus may allow for the indirect detection of many DM models which would otherwise be helicity-suppressed.

Importantly, the decay of the W and Z gauge bosons inevitably leads to the production of secondary annihilation products, including gamma rays, hadrons, charged

leptons and neutrinos, allowing multimessenger searches. Note particularly, that even for DM models designed to be leptophilic, production of hadrons is unavoidable. (In fact, even for models in which on-shell production of W or Z gauge bosons is kinematically forbidden, some minimal hadron production is inescapable, due to loop processes, or the exchange of off-shell W or Z bosons.)

In this paper, we examine a simple example of a model which has a helicity-suppressed $2 \to 2$ cross section, provided by Ref. [29,30]. We shall show that in this model, the cross section required to produce positrons in sufficient quantity to account for the observed excess will lead to overproduction of antiprotons and gamma rays, and as such is ruled out as an explanation of the observed positron anomalies. Though our calculation is performed for the reference scenario of Ref. [29,30], we expect this conclusion to hold for all scenarios in which the dominant positron contributions arise from the 3-body W/Z-bremsstrahlung final states.

We calculate the spectra of both primary and secondary particles from unsuppressed electroweak-bremsstrahlung annihilation processes, and calculate the expected spectra and fluxes at Earth for a given annihilation cross section. We compare the Earthly fluxes with observational data to determine an upper limit on the annihilation cross section. While our analysis techniques are conservative, there are large astrophysical uncertainties in the propagation of charged particles through galactic magnetic fields, and in the DM density profile which probably contains substructure. A rigorous treatment of these effects is beyond the scope of this work. Consequently, our constraints are illustrative of the upper limit on the cross section, but not robust.

II. MODEL

The example model we investigate is the Majorana DM version of the leptophilic model proposed in [29]. Here, the DM consists of a gauge-singlet Majorana fermion χ which annihilates to leptons via the interaction term

$$f(\nu\ell^-)_L \varepsilon \begin{pmatrix} \eta^+ \\ \eta^0 \end{pmatrix} \chi + \text{H.c.} = f(\nu_L \eta^0 - \ell_L^- \eta^+)\chi + \text{H.c.}, \tag{1}$$

where f is a coupling constant, ε is the $SU(2)$-invariant antisymmetric matrix, and (η^+, η^0) form the new $SU(2)$ doublet scalar which mediates the annihilation. For simplicity, we consider a coupling to the first generation of leptons only, and set $f = 0$ for coupling to the $(\nu_\mu \mu^-)_L$ and $(\nu_\tau \tau^-)_L$ doublets. As described in [18,19], the p-wave contribution to the lowest-order annihilation process $\chi\chi \to e^+ e^-$ is suppressed by $v_\chi^2 \sim 10^{-6}$, while the s-wave contribution is proportional to $(m_l/M_\chi)^2$. This cross section is given by

$$v\sigma = \frac{f^4 v^2}{24\pi M_\chi^2} \frac{1+\mu^2}{(1+\mu)^4}, \tag{2}$$

where $m_l \simeq 0$ and $M_{\eta^\pm} = M_{\eta^0}$ have been assumed, and $\mu = M_\eta^2/M_\chi^2$. The helicity-suppressed s-wave term is absent in the $m_l = 0$ limit, leaving only the v_χ^2-suppressed p-wave term.

While it is well known that photon bremsstrahlung $\chi\chi \to e^+ e^- \gamma$ can lift this suppression [15–17], Refs. [18,19] have shown that this is also the case for the electroweak bremsstrahlung channels $\chi\chi \to e^+ e^- Z$, $\nu_e \bar{\nu}_e Z$, $e^+ \nu_e W^-$, $e^- \bar{\nu}_e W^+$. For both W/Z and γ bremsstrahlung, the effect is most significant where the DM mass is nearly degenerate with the mass of the boson which mediates the annihilation process. In the high-energy limit, where the W/Z masses are negligible, the cross sections for W/Z bremsstrahlung reduce to that for γ bremsstrahlung, modulo different coupling constants. However, the respective sizes of the electromagnetic and electroweak coupling constants imply that the W/Z-strahlung cross section is a factor of several larger than that for γ-strahlung,

$$\sigma_{e^+\nu_e W^-} = \sigma_{e^-\bar{\nu}_e W^+} = \frac{1}{2\sin^2\theta_W} \sigma_{e^+e^-\gamma}, \tag{3}$$

$$\sigma_{\bar{\nu}_e \nu_e Z} = \frac{1}{4\cos^2\theta_W \sin^2\theta_W} \sigma_{e^+e^-\gamma}, \tag{4}$$

$$\sigma_{e^+e^-Z} = \frac{(\frac{1}{2} - \sin^2\theta_W)^2}{\cos^2\theta_W \sin^2\theta_W} \sigma_{e^+e^-\gamma}, \tag{5}$$

and thus

$$v\sigma_{W/Z\text{-strahlung}} = 6.16 v\sigma_{e^+e^-\gamma}. \tag{6}$$

At lower energies, the phase space for W/Z bremsstrahlung is somewhat reduced due to the effects of the finite W/Z masses.

The bremsstrahlung cross section dominates over that for the lowest-order $2 \to 2$ process, provided that M_η does not greatly exceed M_χ. The ratio $R_W = v\sigma_{e^+\nu_e W^-}/(v\sigma_{e^+e^-})$ was plotted in Ref. [18], and is largest for $\mu = (M_\eta/M_\chi)^2 = 1$. However, the W-strahlung process dominates over the $2 \to 2$ annihilation even if a mild hierarchy between M_χ and M_η is assumed, with $R_W > 1$ for $\mu \lesssim 10$. Therefore, when $\mu \lesssim 10$, production of mono-energetic leptons will be subdominant to particles produced in the 3-body processes (both primary and through gauge boson decay), a feature which must be accounted for when analyzing astrophysical signatures of these models.

We use the cross sections calculated in [16–18] in combination with the PYTHIA code [31,32] to determine the spectra of gamma rays, electrons, protons, and their antiparticles, per annihilation to the five 3-body final states

listed above (one electromagnetic bremsstrahlung and four electroweak bremsstrahlung processes). After accounting for propagation effects for the charged particles, we constrain these cross sections by comparing the observed flux with the calculated annihilation signal.

Although the spectra of annihilation products which we show are unique to the particular model we have chosen, we expect the results to apply qualitatively to any model where W/Z-bremsstrahlung is the dominant annihilation mode (i.e., where helicity suppression of the $2 \to 2$ s-wave is lifted by electroweak bremsstrahlung).

III. CROSS SECTION CHANNEL

As mentioned, the model we examine is leptophilic in the $2 \to 2$ process, and therefore has five 3-body bremsstrahlung channels, $\chi\chi \to e^+e^-Z$, $\nu_e\bar{\nu}_eZ$, $e^+\nu_eW^-$, $e^-\bar{\nu}_eW^+$, $e^+e^-\gamma$, which simultaneously contribute to the DM annihilation fluxes. The cross sections and spectra for the electroweak channels are specified in Ref. [18], while those for the electromagnetic channel are given in Refs. [16,17]. The total bremsstrahlung cross section is given by the sum

$$v\sigma_{\rm Brem} = v\sigma_{e^+e^-Z} + v\sigma_{\nu_e\bar{\nu}_eZ} + v\sigma_{e^+\nu_eW^-} + v\sigma_{e^-\bar{\nu}_eW^+} + v\sigma_{e^+e^-\gamma}. \quad (7)$$

The total bremsstrahlung cross section is a factor of $\sim$7.2 larger than that for photon bremsstrahlung alone, due to the four W/Z channels, which are governed by somewhat larger coupling constants.

We shall consider parameters for which the bremsstrahlung channels dominate the total cross section, so that $v\sigma_{\rm Brem} \simeq v\sigma_{\rm total}$. We define the "branching ratio" for an individual channel $i \in \{e^+e^-Z, \nu_e\bar{\nu}_eZ, e^+\nu_eW^-, e^-\bar{\nu}_eW^+, e^+e^-\gamma\}$ as

$$BR_{\rm Brem}(i) = \frac{v\sigma_i}{v\sigma_{\rm Brem}}. \quad (8)$$

The spectrum per annihilation, for any given annihilation product, $k \in \{\gamma, e^-, e^+, \nu, \bar{\nu}, p, \bar{p}\}$, is then given by

$$\left.\frac{dN_k}{dE_k}\right|_{\rm Brem} = \sum_i BR_{\rm Brem}(i) \left.\frac{dN_k}{dE_k}\right|_{{\rm per}\ \chi\chi\to i}. \quad (9)$$

Here, $\frac{dN_k}{dE_k}|_{{\rm per}\ \chi\chi\to i}$ is the spectrum per annihilation for a given channel. The spectra for γ, $e^\pm$, ν and $\bar{\nu}$ include primary annihilation products and secondary annihilation products produced by gauge boson fragmentation. The spectra for p and $\bar{p}$ arise exclusively from gauge boson fragmentation. The branching ratios and spectra depend on the parameter $\mu = (M_\eta/M_\chi)^2$. However, as long as the 3-body final states remain the dominant channel, the spectra (and thus the final results) have little dependence on this parameter. We show results for $\mu = (M_\eta/M_\chi)^2 = 1.2$, but results remain qualitatively unchanged when bremsstrahlung channels dominate over $2 \to 2$ processes.

Finally, the flux of a given annihilation product is schematically

$$\frac{d\phi_k}{dE_k} \propto v\sigma_{\rm Brem} \left.\frac{dN_k}{dE_k}\right|_{\rm Brem}. \quad (10)$$

The detailed evaluation of these annihilation spectra is given below.

IV. ANNIHILATION SPECTRA

In order to place constraints on the cross section, we need the spectrum of stable particles (ν, e^-, p and their antiparticles, plus γ) produced per DM annihilation. As an example, we describe how we determine the spectrum of antiprotons per $\chi\chi \to \nu_e e^+ W^-$ event; the technique is very similar for other secondary particles, and other electroweak-bremsstrahlung annihilation channels. These partial spectra are then summed to form $\frac{dN_k}{dE_k}|_{\rm Brem}$.

We use the PYTHIA code [31,32] to find the spectrum of antiprotons per W^- decay, $dN_{\bar{p}}/dE|_{W\ {\rm decay}}$. We produce a W^- boson in its rest frame by colliding an antimuon with a muon neutrino, with center of mass energy M_W, and turning off all processes other than $\mu^\pm\nu_\mu(\bar{\nu}_\mu) \to W^\pm$. (Similarly, to produce the Z boson, we collide a e^+e^- pair at CoM energy M_Z, leaving Z production as the only active process.) Unstable W^- decay products (mainly pions) themselves decay, finally leaving only neutrinos, electrons, protons and their antiparticles, plus gamma rays in the final state. These stable particles are placed in 2000 logarithmically-spaced energy bins. The final spectrum is found by averaging the PYTHIA spectra over 10 000 such events.

We use this energy spectrum, in combination with the W^- (or Z) energy distribution per annihilation, $dN_W/d\gamma = (1/v\sigma)(dv\sigma/d\gamma)$, where $\gamma = E_W/M_W$, to find the antiproton energy-spectrum per annihilation in the lab frame (see Appendix of [19] for a derivation)

$$\frac{dN_{\bar{p}}(E')}{dE'} = \frac{1}{2}\int_1^\infty \frac{d\gamma}{\sqrt{\gamma^2-1}} \frac{dN_W}{d\gamma} \int_{E_-}^{E_+} \frac{dE}{p} \frac{dN_{\bar{p}}}{dE}, \quad (11)$$

with $p = \sqrt{E^2 - m_{\bar{p}}^2}$, $\beta\gamma = \sqrt{\gamma^2-1}$, and $E_\pm = \gamma E' \pm \beta\gamma p'$. Or equivalently,

$$\frac{dN_{\bar{p}}(E')}{dE'} = \frac{1}{2}\int_{m_{\bar{p}}}^\infty \frac{dE}{p} \frac{dN_{\bar{p}}}{dE} \int_{\gamma_-}^{\gamma_+} \frac{d\gamma}{\sqrt{\gamma^2-1}} \frac{dN_W}{d\gamma}, \quad (12)$$

with $\gamma_\pm = (EE' \pm pp')/m_p^2$ and $p' = \sqrt{E'^2 - m_p^2}$. In the case of the gamma-ray, electron, positron, and neutrino spectra, we add the spectrum of primary annihilation products to the spectrum of secondaries from W decay, calculated as above.

Figure 1 shows the total gamma-ray spectrum, as well as the relative contributions from primary and secondary annihilation products, clearly showing that the secondary gamma rays are subdominant, except at low energy.

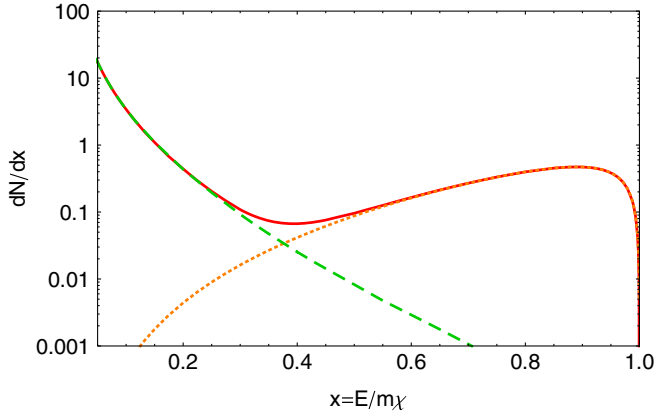

FIG. 1 (color online). Contributions to the gamma-ray spectrum per annihilation, $\frac{dN_\gamma}{dE}|_{\rm brem}$, from primary production in photon bremsstrahlung (dotted, orange), and W/Z decay products (dashed, green), for $M_\chi = 300$ GeV and $M_\eta^2/M_\chi^2 = 1.2$. The total gamma-ray spectrum is also shown (solid, red).

Figure 2 shows the same information for the positron spectra, including the relative contributions to the primary positron spectrum from photon bremsstrahlung and electroweak bremsstrahlung, as well as the secondary positrons produced via gauge boson decay. In Fig. 3, we show the total spectra per annihilation for electrons, neutrinos, protons, and gamma rays. Note that the electron/positron spectra from W/Z and photon bremsstrahlung have differing kinematic cutoffs due to the masses of the $W^\pm$ and Z bosons, leading to a kink near the endpoint in the electron/positron spectra. This feature is absent from the neutrino

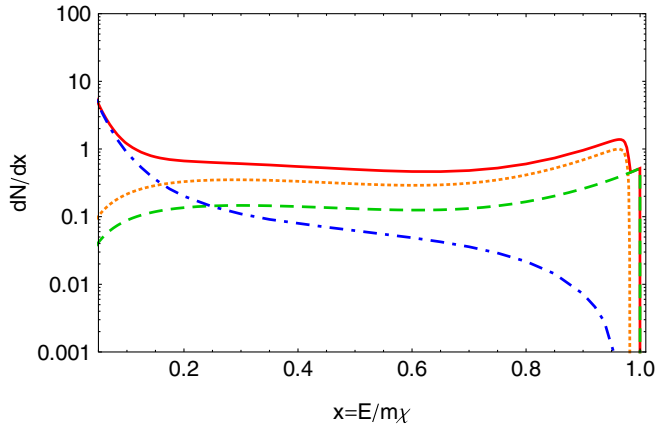

FIG. 2 (color online). Contributions to the positron spectrum per annihilation, $\frac{dN_{e^+}}{dE}|_{\rm brem}$, from primary production in electroweak bremsstrahlung channels (dotted, orange), primary production in the photon bremsstrahlung channel (dashed, green) and W/Z decay products (dot-dashed, blue), for $M_\chi = 300$ GeV and $(M_\eta/M_\chi)^2 = 1.2$. The total positron spectrum is also shown (solid, red). Note that the positron spectra from electroweak and photon bremsstrahlung have differing kinematic cutoffs due to the masses of the $W^\pm$ and Z bosons.

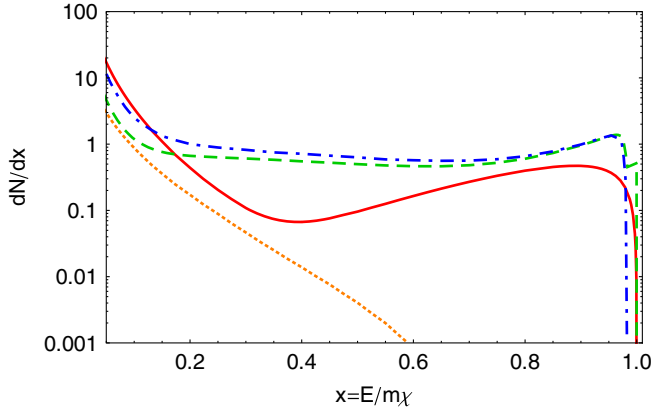

FIG. 3 (color online). Spectrum per annihilation of photons (solid, red), protons (dotted, orange), electrons (dashed, green) and neutrinos (dot-dashed, blue), for $M_\chi = 300$ GeV and $M_\eta^2/M_\chi^2 = 1.2$. For protons, E is the kinetic energy. By CP-invariance, the particle and antiparticle spectra are the same, and antiparticles are not included in this figure. Note that the neutrino spectrum includes primary electron neutrinos, and all flavors of secondary neutrinos.

spectrum, as there is no contribution from photon bremsstrahlung. The neutrino spectrum includes contributions from primary electron neutrinos, and all flavors of secondary neutrinos from $W^\pm/Z$ decay. (The flavor ratios of primary neutrino production are model-dependent, given by $f_e^2{:}f_\mu^2{:}f_\tau^2$. We have assumed $f_\mu = f_\tau = 0$.)

It is illuminating to compare our spectra to those for annihilation to a pair of gauge bosons. The photon spectrum for the WIMP annihilation channel $\chi\chi \to W^+W^-$, shown, for example, in Fig. 1 of Cembranos *et al.* [33], has a somewhat softer gamma spectrum, while we have a somewhat harder spectrum with more higher-energy photons. This is to be expected, as gamma rays in Ref. [33] arise only from decay of mono-energetic W bosons ($E_W = M_\chi$), while the photon-bremsstrahlung process contributes a harder primary gamma-ray spectrum. The reverse holds true for the proton spectra, as our 3-body W/Z-bremsstrahlung process results in a broad distribution of W energies (the spectrum is shown in Fig. 3 of Ref. [18]). In addition, the electron and neutrino spectra resulting from the $\chi\chi \to W^+W^-$ process would be quite different to those for electroweak bremsstrahlung, given that for the latter it is the primary leptons (not the secondaries from W/Z fragmentation) that make the dominant contribution. Of course, the spectra of charged particles observed at Earth will differ from that at production, due to the effect of energy-loss processes during propagation. We address these effects in the following section.

V. CONSTRAINTS

In this section, we place conservative upper limits on the thermally averaged self-annihilation cross section,

$\langle \upsilon\sigma\rangle_{\rm Brem} \simeq \langle \upsilon\sigma\rangle_{\rm total}$, for the leptophilic model described above. We do this by following the same technique as in, for example, [27,34,35]. We compare the various predicted fluxes for a particular DM annihilation channel with the relevant observational flux measurements. We make the conservative assumption that the entire observed flux comes from DM annihilation; in reality, astrophysical backgrounds are likely to contribute a large fraction of the observed fluxes. The upper limit on the cross section is then determined such that the DM annihilation does not exceed any of the observed fluxes.

In calculating the constraints on $\langle \upsilon\sigma\rangle_{\rm Brem}$, we utilize the isotropic extragalactic gamma-ray flux measured by the Fermi collaboration [36], the very-high-energy gamma-ray flux from H.E.S.S. [37], the positron fraction from the PAMELA collaboration [4], the Fermi $e^+ + e^-$ flux [7], as well as the antiproton flux and antiproton-to-proton ratios updated by the PAMELA collaboration in Ref. [5]. Wherever uncertainties in the flux are presented, we use the 1-σ upper limit. Throughout, we use the commonly-adopted Navarro, Frenk and White (NFW) DM density profile [38], with local DM density given by $\rho_\odot = 0.39\ {\rm GeV/cm^{-3}}$ [39].[1] We properly account for proton and electron diffusion and energy loss as detailed below.

A. Gamma rays

The isotropic diffuse gamma-ray flux will have contributions from both galactic and extragalactic DM annihilation. Although the galactic signal is expected to have a large directional dependence, there will be an underlying isotropic component [43]. We include both contributions when computing constraints, though the galactic flux dominates over the extragalactic for the parameters of interest. In order to calculate the cosmic annihilation signal, we follow the technique set out in Refs. [44,45], while adopting the notation of [35,43].

The isotropic gamma-ray flux from DM annihilations throughout the Universe is given by

$$\frac{d\Phi_\gamma}{dE} = \frac{\langle \upsilon\sigma\rangle}{2}\frac{c}{4\pi H_0}\frac{\rho_{\rm av}^2}{M_\chi^2}\int_0^{z_{up}}\frac{f(z)(1+z)^3}{h(z)} \times \frac{dN_\gamma(E')}{dE'}e^{-\tau(z,E)}dz, \quad (13)$$

where $H_0 = 70\ {\rm km\,s^{-1}\,Mpc^{-1}}$ is the Hubble parameter, $\rho_{\rm av}$ is the average DM density in the Universe, and $h(z) = [(1+z)^3\Omega_{\rm DM} + \Omega_\Lambda]^{1/2}$. We assume $\Omega_{\rm DM} = 0.3$, $\Omega_\Lambda = 0.7$. The energy at production is E', and the redshifted energy is $E = E'/(1+z)$. We use the optical depth $\tau(z, E)$ from [44], which accounts for attenuation of gamma rays as they propagate through the Universe. The factor $f(z)$ accounts for the clustering of DM, which gives an enhancement of the annihilation signal relative to a universe in which matter was distributed homogeneously. Following [43], we parametrize the redshift dependence as $\log_{10}(f(z)/f_0) = 0.9[\exp(-0.9z) - 1] - 0.16z$. There is some debate as to the overall normalization of $f(z)$. We adopt the NFW profile, which gives $f_0 \simeq 5\times 10^4$. This is a conservative choice for $f(z)$, and inclusion of enhancements due to subhalos would only strengthen our results. See Ref. [46] for a recent discussion of the clustering factor. Our choice for $f(z)$ closely corresponds to one of the smallest examples given there.

For Galactic annihilation, we again follow the technique of, e.g., [35,43]. The flux of gamma rays per steradian from Galactic DM annihilation, in a direction at an angle ψ from the Galactic Center, is given by

$$\frac{d\Phi_\gamma}{dE} = \frac{1}{2}\frac{\langle \upsilon\sigma\rangle}{4\pi M_\chi^2}\frac{\mathcal{J}(\psi)}{\rm J_0}\frac{dN_\gamma}{dE}, \quad (14)$$

where

$$\mathcal{J}(\psi) = {\rm J_0}\int_0^{\ell_{\rm max}}\rho^2\left(\sqrt{R_{\rm sc}^2 - 2\ell R_{\rm sc}\cos\psi + \ell^2}\right)d\ell \quad (15)$$

is the integral along the line of sight of the DM density squared. ${\rm J_0} = 1/[8.5\ {\rm kpc}\times(0.3\ {\rm GeV\,cm^{-3}})^2]$ is an arbitrary normalization constant used to make $\mathcal{J}(\psi)$ dimensionless; it cancels from our final expression for the gamma-ray flux. Since we are calculating the isotropic signal, we use the minimum value for $\mathcal{J}(\psi)$, once again adopting the NFW profile.

The Extragalactic Gamma-Ray Background (EGB) reported by Fermi in [36] is the isotropic component of the diffuse gamma-ray flux, with a number of potential contributing sources. It is obtained by subtracting the components of the gamma-ray flux with known origin from the total flux, observed away from the Galactic disk (Galactic latitude $|b| \geq 10^\circ$). Hence, it is a flux likely to contain a contribution from either Galactic or extragalactic DM annihilation. We compare our calculated isotropic signal, from both cosmic and Galactic annihilation, to this isotropic flux. We do this for each data energy bin, integrating the signal over the width of each bin in turn.

We also compare the DM annihilation signal with H.E.S.S. observations of the very-high-energy gamma-ray flux from an angular region of 1° around the Galactic Center, excluding the Galactic Plane [37]. These observations have both advantages and disadvantages when compared with the Fermi EGB observations. First, the two data sets cover different energy regimes. The H.E.S.S. data begin at around 300 GeV, and so are unable to constrain the cross section at lower DM masses. Conversely, Fermi EGB data end at 100 GeV, such that constraints on the cross section for larger DM masses are based on comparisons of the observed flux with the tail end of the annihilation spectrum, leading to relatively weak constraints. In addition, the two data sets are from drastically different

[1] $\rho_\odot = 0.389 \pm 0.025$ (1-σ) [39], but could be a factor of $\sim$2 higher or lower [40–42].

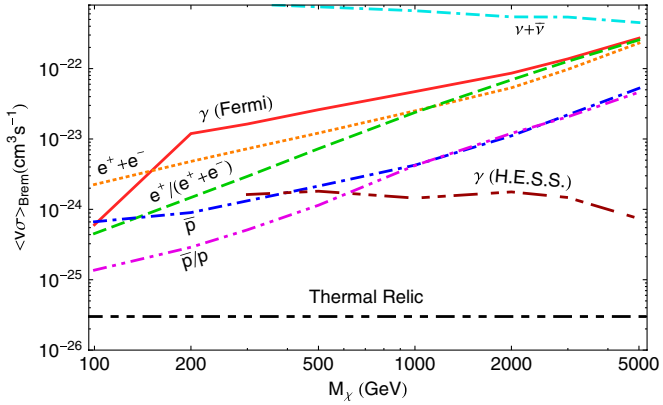

FIG. 4 (color online). Upper limits on $\langle v\sigma \rangle_{\rm Brem}$ using the "med" diffusion parameter set. Shown are constraints based on the Fermi EGB (solid, red), $e^+ + e^-$ flux (dots, orange), $e^+/(e^+ + e^-)$ ratio (dashes, green), $\bar{p}$ flux (dot-dashes, blue), $\bar{p}/p$ ratio (dot-dot-dashes, magenta), H.E.S.S. gamma rays (dot-dot-dot-dashes, maroon), and neutrinos (dot-dash-dashes, cyan). Also shown for comparison is the expected cross section for thermal relic dark matter, 3×10^{-26} cm^3/s (dot-dot-dash-dashes, black).

observation regions. The expected isotropic DM signal is relatively small, leading to weaker constraints from the Fermi data; however, this is balanced by the small uncertainty between the various DM density profiles for this region. The opposite holds true for the H.E.S.S. observation region, where there is a large expected DM signal, large background flux, and a very large uncertainty between competing density profiles, since the observation region is small and close to the Galactic Center. While we report results using the NFW profile, these would be weakened by well over an order of magnitude if an isothermal profile were adopted.

For these reasons it makes sense to constrain the annihilation rate using both data sets, emphasizing that while we find that the H.E.S.S. constraints are significantly stronger, they are subject to larger uncertainties. We follow the same technique as earlier, treating the flux from the Source region in Ref. [37] as an upper limit on the annihilation flux calculated using Eq. (15) for each reported energy bin, allowing us to place an upper limit on $\langle v\sigma \rangle$ as a function of the DM mass. We again present results using the NFW profile, utilizing the average of $\mathcal{J}(\psi)$ over the observation region as reported in Ref. [37], $\mathcal{J}_{\rm av} = 1604$.

Our resulting upper limits on $\langle v\sigma \rangle$ using both Fermi EGB and H.E.S.S. data are reported in Fig. 4.

B. Electrons and positrons

The flux of positrons (or electrons) at Earth from DM annihilation depends both on the propagation of the positrons through the turbulent galactic magnetic fields, and energy losses of the particles. One can solve the applicable diffusion-energy loss equation to find a semi-analytic form for the positron flux at Earth. We adopt the same notation and set of assumptions as in, e.g., Ref. [47], which gives

$$\frac{d\Phi_e(E)}{dE} = \frac{\langle v\sigma \rangle \rho_\odot^2 v}{8\pi M_\chi^2 b(E)} \int_E^{M_\chi} dE' \frac{dN_e}{dE} I(\lambda_D(E, E')), \quad (16)$$

where $\rho_\odot$ is the local DM density, $b(E)$ and $I(\lambda_D(E, E'))$ are the energy loss and "halo function" parameters, respectively, and $\lambda_D(E, E')$ is the diffusion length between the two energies E and E'. The energy loss of the positrons as they propagate through the Galactic medium is mainly due to synchrotron radiation and inverse Compton scattering, and is characterized by $b(E) \approx 10^{-16}(E/\text{GeV})^2$ GeV s^{-1}. The "halo function" $I(\lambda_D(E, E'))$ is an astrophysical parametrization which encodes the dependence of the flux on the DM density profile, and on the model of positron diffusion due to Galactic magnetic fields. There is a degree of uncertainty in this function, and so we choose the "medium" diffusion parameter set (while also showing results in the "min" and "max" scenarios), and as usual, the NFW DM density profile. We use the numerical fit to $I(\lambda_D(E, E'))$ from [47].

Our signal is then compared with the total $e^+ + e^-$ flux reported by the Fermi collaboration [7] to find an upper limit on $\langle v\sigma \rangle$, by demanding that the signal integrated over the width of an energy bin be less than the total observed flux in that bin,

$$(\Phi_{e^+} + \Phi_{e^-})^{\rm signal} = 2\Phi_{e^+}^{\rm signal} \lesssim \Phi_{e^+ + e^-}^{\rm obs}. \quad (17)$$

We can also combine our positron flux with the Fermi data to find the positron fraction from DM annihilation. We compare this with the PAMELA data [4] for the positron fraction (f_{e^+}) to find an alternative upper limit on $\langle v\sigma \rangle$ by demanding

$$\frac{\Phi_{e^+}}{\Phi_{e^+ + e^-}^{\rm obs}} \leq f_{e^+}. \quad (18)$$

We compare the DM-related positron fraction with the observed PAMELA fraction in each of the four energy bins where the Fermi energy range overlaps the PAMELA energy range, integrating the DM-signal and observed Fermi fluxes over the width of the PAMELA energy bins. For this, we use the simple power-law fit to the Fermi data, valid between around 20 GeV and 1 TeV [10],

$$\frac{d\Phi_{e^+ + e^-}^{\rm obs}}{dE} = (175.40 \pm 6.09) \times 10^{-4}\ (\text{GeV cm}^2\,\text{s sr})^{-1} \times (E/\text{GeV})^{(-3.045 \pm 0.008)}. \quad (19)$$

Results are reported in Fig. 4, while results in the "minimum" and "maximum" diffusion scenarios are shown in Fig. 5.

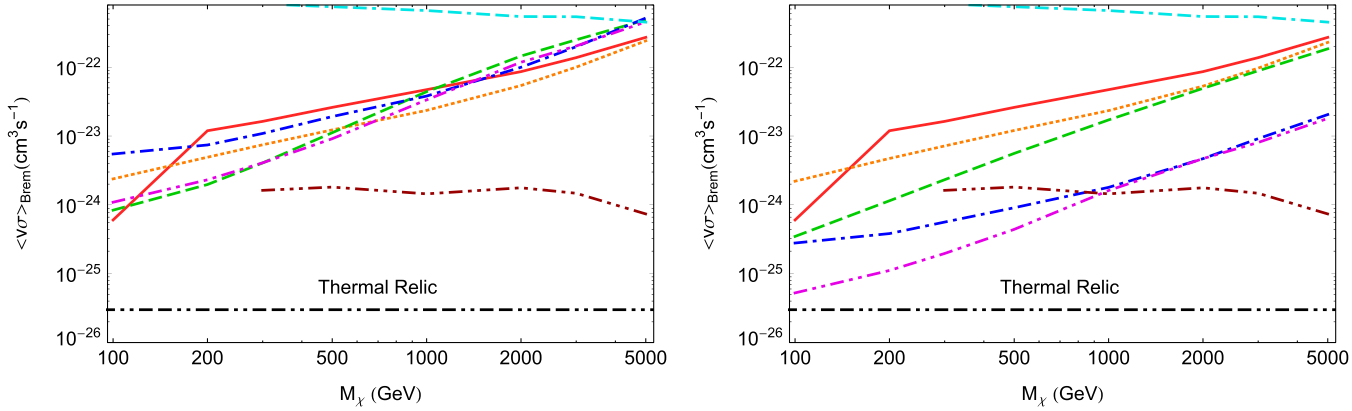

FIG. 5 (color online). As for Fig. 4, using the "min" (left) and "max" (right) diffusion parameter sets.

C. Protons and antiprotons

The antiproton (or proton) flux at Earth has a similar functional form to that for positrons, except that the energy losses for the antiprotons as they propagate to Earth are negligible, since $m_p \gg m_e$. (Note that although energy loss is negligible, diffusion is not.) Because the energy for the antiprotons is the same as the injection energy, there is no need for an integration over energies E' at production. (Energy loss due to scattering interactions or solar modulation are relevant only at low energies.) We again use the semi-analytic function from [47] to calculate the proton and antiproton signals at Earth from DM annihilation,

$$\frac{d\Phi_p(K)}{dK} = \frac{\langle v\sigma\rangle \rho_\odot^2 v}{8\pi M_\chi^2} R(K), \tag{20}$$

where K is the kinetic energy of the (anti)-proton, and $R(K)$ is an astrophysics parametrization playing a similar role to $I(\lambda_D(E, E'))$ from Sec. V B. Reference [47] provides a numerical fit to $R(K)$ for several sets of propagation parameters, and we again use the "medium" parameter set, with the NFW DM density profile.

We compare our antiproton flux with the total antiproton flux reported by the PAMELA collaboration [5], energy bin by energy bin. We can also constrain the cross section by demanding the ratio $\bar{p}/p$ due to antiprotons from DM annihilation not exceed the PAMELA $\bar{p}/p$ ratio [5,6]. This comparison requires the observed proton flux. Following [27], we use the nucleon flux from [48], $\frac{d\Phi_p^{\rm obs}}{dE} \approx 0.79 \times 1.8(E/\mathrm{GeV})^{-2.7}(\mathrm{cm^2\,s\,GeV})^{-1}$, where 0.79 is the proton fraction of the total nucleon flux. We then simply demand $\Phi_{\bar{p}}/\Phi_p^{\rm obs} \lesssim f_{\bar{p}/p}$, where $f_{\bar{p}/p}$ is the PAMELA antiproton/proton flux ratio given in [5]. Energy bins have been handled in the same way as the positron case, giving us the upper limit on $\langle v\sigma\rangle$ shown in Fig. 4, and results using the "minimum" and "maximum" diffusion parameter sets are shown for comparison in Fig. 5.

D. Neutrinos

Following Ref. [43], we examine the neutrino flux averaged over the entire sky. The dominant contribution to the DM signal will be from Galactic annihilations, and we ignore the subdominant cosmic annihilation signal. We make the approximation that 1/3 of all produced neutrinos will be observed as muon neutrinos,

$$\frac{dN_{\nu_\mu}}{dE} = \frac{1}{3}\frac{dN_\nu}{dE}. \tag{21}$$

Note that the neutrino spectrum in Fig. 3 includes primary electron neutrinos, and all flavors of secondary neutrinos. We then compare the $\nu_\mu + \bar{\nu}_\mu$ signal from DM annihilation with the atmospheric $\nu_\mu + \bar{\nu}_\mu$ flux, using the same technique as Ref. [43]. The calculation of the Galactic neutrino signal proceeds the same as for gamma rays, using Eq. (15) with the neutrino-annihilation spectrum in place of the gamma-ray spectrum.

We average $\mathcal{J}(\psi)$ over the entire sky, and find $\mathcal{J}_{\rm av} \simeq 5$ for the NFW profile. The signal is then compared with the background flux, integrating each over an energy bin width of $\Delta\log_{10}E = 0.3$. As expected, the resulting upper limit on the cross section is significantly weaker than those calculated using the other annihilation products considered, and is only visible in the high-mass region of Fig. 4. Accordingly, the assumptions made in this subsection concerning neutrino flavors are moot.

As an alternative technique, one could calculate the flux of upward-going muons through the Earth induced by neutrinos from DM annihilation, and compare this with limits from the Super-Kamiokande (SuperK) experiment [49]. Reference [50] converts the SuperK limits into an upper limit on the annihilation cross section to a neutrino-antineutrino pair. Comparing this with limits on the same channel from Ref. [43], whose technique we follow, suggests that the limits presented in this work would not be substantially strengthened by the SuperK data set, certainly not to the point where the neutrino constraints on $\langle v\sigma\rangle_{\rm Brem}$ were competitive with any of the stronger bounds.

VI. DISCUSSION

Figure 4 collects our upper limits on the bremsstrahlung cross section $\langle \upsilon\sigma \rangle_{\rm Brem}$, as calculated in the previous sections. The constraint from the antiproton ratio is stronger than that from the positron data by a factor of $\sim$5. Nature provides a unique value for $\langle \upsilon\sigma \rangle$. Therefore, if the bremsstrahlung process saturates the allowed antiproton limit, then the same process produces positrons at a rate down from the observed value by about a factor of five.[2] Conversely, if the observed positron fraction were attributed to the bremsstrahlung process, then the same process would overproduce antiprotons by about a factor of five.

It is important to note that the observed antiproton flux and ratio are well reproduced by standard astrophysical processes, leaving little room for a DM contribution.[3] We have not attempted to model this standard background, so constraints from antiprotons are likely to be significantly stronger than presented here.

Annihilation to $\mu^+\mu^-$ or $\tau^+\tau^-$ is not as helicity-suppressed as to electrons. Even so, the helicity factors which suppress the s-wave are $(m_\mu/M_\chi)^2 \simeq 10^{-7} \times (M_\chi/300\ {\rm GeV})^{-2}$ and $(m_\tau/M_\chi)^2 \simeq 3 \times 10^{-5} \times (M_\chi/300\ {\rm GeV})^{-2}$, which are comparable to the factor by which the p-wave is velocity suppressed, $\upsilon^2 \sim 10^{-6}$. Since bremsstrahlung overcomes both suppressions, it can also be important for annihilation to muons and taus. (And, of course, any helicity suppression is especially stringent for annihilation to ν_μ and ν_τ, as $m_\nu \simeq 0$.) In the case of relatively light DM annihilating to taus, the helicity suppression is not as pronounced. Furthermore, W/Z bremsstrahlung may be kinematically forbidden. In any case, we note that annihilation to τ can never be purely leptophilic, as the τ has significant hadronic decay modes.

Note that in the model we consider, emission of photons or massive gauge bosons can always lift helicity suppression, however, the effect will be much greater in magnitude when the DM and scalar exchange particles are nearly degenerate in mass (such as the co-annihilation region of mSUGRA). In the present work, we consider such a region of parameter space. Specifically, we present results for $\mu = (M_\eta/M_\chi)^2 = 1.2$, though our conclusions remain valid for any value of μ where the bremsstrahlung processes dominate the 2 to 2 body processes. As can be seen in Ref. [18], the rates for these two processes become comparable at $\mu \sim 10$.

Consider now scenarios where DM annihilation to a lepton pair is *not* helicity-suppressed. As examples, one may have Majorana DM annihilating via an exchange of a pseudoscalar or scalar (the latter is still velocity-suppressed at the DM vertex) or Dirac DM annihilating via the exchange of a vector, or one may have scalar DM annihilations. In these cases, there will still be a signal from electroweak bremsstrahlung emission [24,27,28], although it will no longer be the dominant channel. Even so, the W/Z decay products can still lead to restrictive constraints. Reference [27] considered an example (exchange of a scalar) where EW bremsstrahlung makes only a subdominant contribution to the total DM annihilation rate. In this model, the main contribution to the annihilation rate comes from the 2-body annihilation channels, thus the monoenergetic $e^\pm$ and neutrino fluxes dwarf the gauge boson fragmentation products. Nonetheless, Ref. [27] found that the antiproton data still provide the most stringent cross section constraints for certain parameters. Note however, that the models of [24,27] explicitly break gauge invariance. A detailed, model-independent, treatment of weak corrections may be found in Ref. [28].

It should be noted that the results presented here are not due to an exhaustive survey of all possible DM profiles and parameters. Uncertainties arise from the various choices made in order to present illustrative results. In most cases, we have made conservative choices for these parameters such that alterations to these selections should strengthen the results. In calculating the flux of protons, antiprotons, electrons and positrons, all the astrophysical parameters are encoded into a numerically fit function [47] with propagation parameters which are consistent with a ''median'' flux [52]. However, by assuming alternate parameters, e.g., from the ''max'' or ''min'' flux scenarios, our results may be strengthened or weakened by up to an order of magnitude, as shown in Fig. 5. Our conclusions hold in all cases considered, but for the extreme choice of ''min'' diffusion parameter set, where the $e^+/(e^+ + e^-)$ limits become comparable to those for $\bar{p}/p$ and the $e^+ + e^-$ limits become comparable to those for gamma rays.

Obviously, the choice of profile can have a large effect on the parameter ranges, and we have adopted the NFW profile with $\rho_\odot = 0.39\ {\rm GeV/cm^{-3}}$ throughout this work. If one considers nonspherical profiles or dark discs, then the uncertainty in the value of the local DM density may be expanded to accommodate a value between $0.2\ {\rm GeV/cm^{-3}}$ and $0.7\ {\rm GeV/cm^{-3}}$ [40]. Note, however, that changes to the DM profile would move all the predicted fluxes, and thus the corresponding cross section constraints, in the same direction. For the calculation of the extragalactic fluxes, the cosmic source clustering factor [$f(z)$ of Eq. (14)] can vary by an order of magnitude depending on the profile and inclusion or exclusion of subhalos [43] (for example, in the case of the Moore profile [53], our choice for normalization could be increased by a

[2]Note that we have not compared the spectral shapes of the DM signals with those of the observed fluxes, nor tried to *fit* the data.

[3]Reference [51] notes that a highly anisotropic diffusion model, as might be invoked to accommodate galactic winds, may suppress the antiproton flux to a value possibly below the PAMELA flux. We do not consider anisotropic diffusion in this work.

factor of 10 [54]). This would lead to tighter constraints coming from the gamma ray signals.

We have also neglected the signals produced by inverse Compton scattering (gamma rays) and synchrotron radiation (radiowaves) of the electrons and positrons as they propagate in the galaxy (see, e.g., Ref. [55,56]). Note, however, that these effects are properly included in the electron energy-loss formalism we adopt. We expect the gamma rays produced directly from the annihilations to dominate the constraints. Additional gamma rays from inverse Compton would only strengthen our results (but make them less robust).

VII. CONCLUSIONS

If DM is Majorana in nature, then its annihilation to fermions may be suppressed due to helicity considerations. However, when the DM mass is greater than $M_W/2$, both electroweak and photon bremsstrahlung may lift this suppression, thereby becoming the dominant channel for DM annihilation. This permits the indirect detection of models for which the annihilation cross section would otherwise be too suppressed to be of interest. Subsequent decay of the emitted W and Z gauge boson will produce fluxes of electrons, positrons, neutrinos, hadrons, and gamma rays. The aim of the present work has been to study the spectra of these particles as a tool for indirect detection of DM. By comparing these fluxes to cosmic ray data we have been able to constrain the DM annihilation cross section in such models. From these constraints, we find that the observational data pertaining to the flux of antiprotons combined with those of positrons make it difficult for helicity-suppressed $2 \rightarrow 2$ leptophilic DM annihilation to be the source of the recently detected cosmic ray anomalies. For these models, the bremsstrahlung processes dominate. The primary culprit is the hadronization of the gauge bosons, which leads to a significant antiproton flux. This result highlights the difficulty of producing lepton-only final states even in a model expressly designed for just such a purpose with $2 \rightarrow 2$ annihilation.

ACKNOWLEDGMENTS

We thank Sheldon Campbell and Yudi Santoso for helpful discussions. N. F. B. was supported by the Australian Research Council, T. D. J. was supported in part by the Commonwealth of Australia, J. B. D. and T. D. J. were supported in part by the Arizona State University Cosmology Initiative, J. B. D. was supported in part by U.S. Department of Energy, and T. J. W. was supported in part by U.S. Department of Energy Grant No. DE-FG05-85ER40226..

[1] G. Jungman, M. Kamionkowski, and K. Griest, Phys. Rep. **267**, 195 (1996).
[2] G. Bertone, D. Hooper, and J. Silk, Phys. Rep. **405**, 279 (2005).
[3] L. Bergstrom, Rep. Prog. Phys. **63**, 793 (2000).
[4] O. Adriani *et al.* (PAMELA), Nature (London) **458**, 607 (2009); O. Adriani *et al.*, Astropart. Phys. **34**, 1 (2010).
[5] O. Adriani *et al.* (PAMELA Collaboration), Phys. Rev. Lett. **105**, 121101 (2010).
[6] O. Adriani *et al.*, Phys. Rev. Lett. **102**, 051101 (2009).
[7] A. A. Abdo *et al.* (The Fermi LAT), Phys. Rev. Lett. **102**, 181101 (2009); M. Ackermann *et al.* (Fermi LAT Collaboration), Phys. Rev. D **82**, 092004 (2010) arXiv:1008.3999.
[8] F. Aharonian *et al.* (H.E.S.S. Collaboration), Astron. Astrophys. **508**, 561 (2009).
[9] D. Hooper, P. Blasi, and P. D. Serpico, J. Cosmol. Astropart. Phys. 01 (2009) 025; H. Yuksel, M. D. Kistler, and T. Stanev, Phys. Rev. Lett. **103**, 051101 (2009); S. Profumo, arXiv:0812.4457; D. Malyshev, I. Cholis, and J. Gelfand, Phys. Rev. D **80**, 063005 (2009); V. Barger, *et al.*, Phys. Lett. B **678**, 283 (2009); D. Malyshev, J. Cosmol. Astropart. Phys. 07 (2009) 038.
[10] D. Grasso *et al.* (FERMI-LAT), Astropart. Phys. **32**, 140 (2009).
[11] N. J. Shaviv, E. Nakar, and T. Piran, Phys. Rev. Lett. **103**, 111302 (2009); Y. Fujita, *et al.*, Phys. Rev. D **80**, 063003 (2009).
[12] P. Blasi, Phys. Rev. Lett. **103**, 051104 (2009); H. B. Hu, *et al.*, Astrophys. J. **700**, L170 (2009)S. Dado and A. Dar, Mem. Soc. Astron. Ital. **81**, 132 (2010); P. Mertsch and S. Sarkar, Phys. Rev. Lett. **103**, 081104 (2009).
[13] L. Stawarz, V. Petrosian, and R. D. Blandford, Astrophys. J. **710**, 236 (2010); R. Cowsik and B. Burch, arXiv:0905.2136; B. Katz, K. Blum, and E. Waxman, Mon. Not. R. Astron. Soc. **405**, 1458 (2010);.
[14] Y.-Z. Fan, B. Zhang, and J. Chang, Int. J. Mod. Phys. D **19**, 2011 (2010); X.-G. He, Mod. Phys. Lett. A **24**, 2139 (2009).
[15] L. Bergstrom, Phys. Lett. B **225**, 372 (1989); R. Flores, K. A. Olive, and S. Rudaz, Phys. Lett. B **232**, 377 (1989); E. A. Baltz and L. Bergstrom, Phys. Rev. D **67**, 043516 (2003); arXiv:hep-ph/0211325; V. Barger, *et al.*, Phys. Rev. D **80**, 063537 (2009).
[16] T. Bringmann, L. Bergstrom, and J. Edsjo, J. High Energy Phys. 01 (2008) 049.
[17] L. Bergstrom, T. Bringmann, and J. Edsjo, Phys. Rev. D **78**, 103520 (2008).
[18] N. F. Bell, *et al.*, Phys. Lett. B (to be published). While the main point of Ref. [19] was to establish that W/Z-bremsstrahlung contributes an unsuppressed

s-wave amplitude to Majorana dark matter annihilation, we subsequently found some errors in the explicit cross section calculations of Ref. [19]. This reference corrects those errors.

[19] N. F. Bell, *et al.*, Phys. Rev. D **83**, 013001 (2011).
[20] P. Ciafaloni, *et al.*, J. Cosmol. Astropart. Phys. 1106 (2011)018.
[21] X. l. Chen and M. Kamionkowski, J. High Energy Phys. 07 (1998) 001.
[22] V. Berezinsky, M. Kachelriess, and S. Ostapchenko, Phys. Rev. Lett. **89**, 171802 (2002).
[23] M. Kachelriess and P. D. Serpico, Phys. Rev. D **76**, 063516 (2007).
[24] N. F. Bell, *et al.*, Phys. Rev. D **78**, 083540 (2008).
[25] J. B. Dent, R. J. Scherrer, and T. J. Weiler, Phys. Rev. D **78**, 063509 (2008).
[26] P. Ciafaloni and A. Urbano, Phys. Rev. D **82**, 043512 (2010).
[27] M. Kachelriess, P. D. Serpico, and M. A. Solberg, Phys. Rev. D **80**, 123533 (2009).
[28] P. Ciafaloni, *et al.*, J. Cosmol. Astropart. Phys. 03 (2011) 019.
[29] Q.-H. Cao, E. Ma, and G. Shaughnessy, Phys. Lett. B **673**, 152 (2009).
[30] E. Ma, Phys. Rev. Lett. **86**, 2502 (2001).
[31] T. Sjostrand, S. Mrenna, and P. Z. Skands, J. High Energy Phys. 05 (2006) 026.
[32] T. Sjostrand, S. Mrenna, and P. Z. Skands, Comput. Phys. Commun. **178**, 852 (2008).
[33] J. A. R. Cembranos, *et al.*, Phys. Rev. D **83**, 083507 (2011) Additional spectra in great detail, per annihilation channel, can be found in Ref. [55], ;
[34] N. F. Bell and T. D. Jacques, Phys. Rev. D **79**, 043507 (2009).
[35] G. D. Mack, *et al.*, Phys. Rev. D **78**, 063542 (2008).
[36] A. A. Abdo *et al.* (The Fermi-LAT), Phys. Rev. Lett. **104**, 101101 (2010).
[37] A. Abramowski *et al.* (H.E.S.S. Collaboration), Phys. Rev. Lett. **106**, 161301 (2011).
[38] J. F. Navarro, C. S. Frenk, and S. D. M. White, Astrophys. J. **462**, 563 (1996).
[39] R. Catena and P. Ullio, J. Cosmol. Astropart. Phys. 08 (2010)004.
[40] M. Weber and W. de Boer, Astron. Astrophys. Rev. **509**, A25 (2010).
[41] P. Salucci, *et al.*, Astron. Astrophys. Rev. **523**, A83 (2010).
[42] I. Cholis and L. Goodenough, J. Cosmol. Astropart. Phys. 09 (2010) 010.
[43] H. Yuksel, *et al.*, Phys. Rev. D **76**, 123506 (2007); See also J. F. Beacom, N. F. Bell, G. D. Mack, Phys. Rev. Lett. **99**, 231301 (2007).
[44] P. Ullio, L. Bergstrom, J. Edsjo, and C. G. Lacey, Phys. Rev. D **66**, 123502 (2002).
[45] L. Bergstrom, J. Edsjo, and P. Ullio, Phys. Rev. Lett. **87**, 251301 (2001).
[46] A. A. Abdo *et al.* (Fermi-LAT Collaboration), J. Cosmol. Astropart. Phys. 04 (2010) 014.
[47] M. Cirelli, R. Franceschini, and A. Strumia, Nucl. Phys. **B800**, 204 (2008).
[48] K. Nakamura *et al.* (Particle Data Group), J. Phys. G **37**, 075021 (2010).
[49] S. Desai *et al.* (Super-Kamiokande Collaboration), Phys. Rev. D **70**, 083523 (2004); **70**, 109901(E) (2004).
[50] A. E. Erkoca, *et al.*, Phys. Rev. D **81**, 096007 (2010).
[51] P. Grajek and K. Hagiwara, arXiv:1012.0587.
[52] F. Donato, *et al.*, Phys. Rev. D **69**, 063501 (2004).
[53] B. Moore, *et al.*, Mon. Not. R. Astron. Soc. **310**, 1147 (1999).
[54] S. Ando, Phys. Rev. Lett. **94**, 171303 (2005).
[55] M. Cirelli, *et al.*, J. Cosmol. Astropart. Phys. 03 (2011) 051.
[56] R. M. Crocker, *et al.*, Phys. Rev. D **81**, 063516 (2010).